Proximity Biotinylation as a Method for Mapping Proteins Associated with mtDNA in Living Cells

Shuo Han[1], **Namrata D. Udeshi**[2], **Thomas J. Deerinck**[3], **Tanya Svinkina**[2], **Mark H. Ellisman**[3], **Steven A. Carr**[2], and **Alice Y. Ting**[1,4,*]

[1]Departments of Genetics, Biology, and Chemistry, Stanford University, Stanford, CA 94305, USA

[2]Broad Institute of MIT and Harvard, Cambridge, MA 02142, USA

[3]National Center for Microscopy and Imaging Research, University of California at San Diego, La Jolla, CA 92093, USA

SUMMARY

A recurring challenge in cell biology is to define the molecular components of macromolecular complexes of interest. The predominant method, immunoprecipitation, recovers only strong interaction partners that survive cell lysis and repeated detergent washes. We explored peroxidase-catalyzed proximity biotinylation, APEX, as an alternative, focusing on the mitochondrial nucleoid, the dynamic macromolecular complex that houses the mitochondrial genome. Via 1-min live-cell biotinylation followed by quantitative, ratiometric mass spectrometry, we enriched 37 nucleoid proteins, seven of which had never previously been associated with the nucleoid. The specificity of our dataset was very high, and we validated three hits by follow-up studies. For one novel nucleoid-associated protein, FASTKD1, we discovered a role in downregulation of mitochondrial complex I via specific repression of ND3 mRNA. Our study demonstrates that APEX is a powerful tool for mapping macromolecular complexes in living cells, and can identify proteins and pathways that have been missed by traditional approaches.

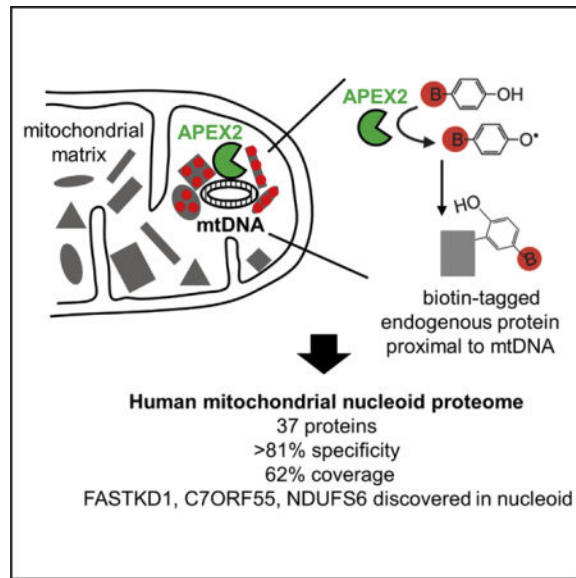## Graphical abstract

---

*Correspondence: ayting@stanford.edu.
[4]Lead Contact

Human mitochondrial nucleoid proteome
37 proteins
>81% specificity
62% coverage
FASTKD1, C7ORF55, NDUFS6 discovered in nucleoid

INTRODUCTION

The mitochondrial genome, or mtDNA, encodes 37 genes and is compacted into a nucleoprotein complex within the mitochondrial matrix called the mitochondrial nucleoid. The nucleoid houses proteins involved in mtDNA replication, maintenance, and transcription, and is also thought to include peripheral factors that enable crosstalk between the mitochondrial genome and a range of mitochondrial and cellular processes, including oxidative phosphorylation, mitochondrial biogenesis, and nuclear transcription (Gilkerson et al., 2013). Dysfunction of known nucleoid proteins leads to a spectrum of human mitochondrial diseases (Copeland, 2012).

Although understanding the composition of the mitochondrial nucleoid is essential to understanding mitochondrial biology, the nucleoid has been difficult to characterize because it cannot be purified by traditional biochemical fractionation. The nucleoid is not surrounded by a membrane, and is thought to be a dynamic structure with transiently associated components (Gilkerson et al., 2013). Previous efforts to map the nucleoid by mass spectrometry (MS) have used either crosslinking followed by fractionation (Bogenhagen et al., 2008; Kaufman et al., 2000; Rajala et al., 2015) or immunoprecipitation of known nucleoid proteins (He et al., 2012; Rajala et al., 2015; Wang and Bogenhagen, 2006). The former approach retrieves contaminants, including even cytosolic and nuclear proteins (Bogenhagen et al., 2008; Rajala et al., 2015) (Figure S1A), while the latter misses transient interaction partners that do not survive cell lysis and detergent washes. Consequently, the previous datasets trade specificity for depth of coverage, or vice versa (Figure S1A), and there is poor consensus between them (Figure S1B).

An alternative approach to studying the mitochondrial nucleoid is to use recently developed proximity biotinylation methods (Loh et al., 2016; Rhee et al., 2013; Roux et al., 2012) to tag endogenous nucleoid components in live cells and then use MS to determine the identities of the tagged proteins (Figure 1A). The advantages of such an approach are

potentially higher specificity, due to avoidance of crosslinking and fractionation that could introduce contaminants, and greater sensitivity, due to detection of transient or weakly associated nucleoid components that remain with the nucleoid in live cells but are lost during pull-downs. We previously used peroxidase proximity labeling with ascorbate peroxidase (APEX) to tag the proteomes of the entire mitochondrial matrix space (Rhee et al., 2013) and intermembrane space (IMS) (Hung et al., 2014) in live cells. The proteomes of 495 and 127 proteins, respectively, were highly specific (<6% false discovery rates) and had reasonable coverage (85% and 65%, respectively). The mitochondrial nucleoid, however, represents a much greater challenge for APEX methodology. Whereas the matrix and IMS are membrane-enclosed organelles, the nucleoid is an open, non-membrane-enclosed macromolecular complex.

By using a Twinkle-APEX2 genetic fusion to target the peroxidase to mitochondrial nucleoids of living human fibroblasts, and performing a 1-min biotinylation reaction, we enriched a nucleoid proteome of 37 proteins. Only mitochondrial proteins are present in this list (i.e., no cytosolic or nuclear contaminants) and 30 (81%) are known nucleoid proteins. Interestingly, 12 proteins (32%) in our dataset have functions related to RNA; several of these were missed by previous immunoprecipitation-based nucleoid studies (He et al., 2012; Wang and Bogenhagen, 2006), or discarded as non-mitochondrial contaminants in the cross-linking-based studies (Bogenhagen et al., 2008) due to the high false-positive rates of these datasets. We followed up on one of these proteins, FASTKD1, and found that it specifically downregulates one of the 13 mRNAs encoded by mtDNA: ND3, a subunit of complex I. Our study demonstrates the value of proximity biotinylation as a complementary approach to traditional immunoprecipitation and formaldehyde crosslinking to elucidate new proteins and functions of the mitochondrial nucleoid.

RESULTS

Targeting APEX to the Mitochondrial Nucleoid

We fused APEX2, the newer and more catalytically active version of APEX (Lam et al., 2015), to two well-characterized mitochondrial nucleoid proteins that have previously been tagged with GFP: the DNA helicase Twinkle (Rajala et al., 2014; Spelbrink et al., 2001) (Figure 1B) and the mitochondrial transcription factor TFAM (Brown et al., 2011). Although both APEX2 fusion constructs localized correctly to mitochondria, only Twinkle-APEX2 gave the expected punctate staining pattern within mitochondria (Figure S1C). By contrast, overexpressed TFAM-APEX2 filled the entire mitochondrion (Figure S1C). Co-staining with anti-DNA antibody to visualize mtDNA-containing nucleoids showed good overlap with Twinkle-APEX2 (Figure 1C), but not TFAM-APEX2.

To minimize Twinkle-APEX2 expression levels, we selected HEK cells stably expressing Twinkle-APEX2 after lentiviral transduction. These stable cells showed mtDNA levels similar to those of untransfected HEK cells in a qPCR assay (Figure S1F), suggesting that Twinkle-APEX2 at these levels does not perturb mitochondrial physiology. This result also agrees with previous literature (Wanrooij et al., 2007).

To characterize Twinkle-APEX2 in greater detail, we took advantage of APEX2's ability to generate contrast for electron microscopy (EM) (Lam et al., 2015; Martell et al., 2012). HEK 293T cells stably expressing Twinkle-APEX2 were fixed, stained with diaminobenzidine and osmium, and processed for EM. In Figure 1D, APEX2-tagged nucleoids appear as dark regions, 150–200 nm in diameter, within the mitochondrial matrix. In most fields of view, the nucleoid abuts the IMS and outer mitochondrial membrane (OMM). Cristae surrounding each nucleoid appear distorted, as if displaced by the nucleoprotein complex. These observations are consistent with previous super-resolution fluorescence studies (Kopek et al., 2012), which found that nucleoids occupy "cristae-free" regions and only contact specific cristae parts (tips, sides, and junctions).

Separate from our application to proteomics here, the Twinkle-APEX2 fusion construct may be a valuable tool for high-resolution imaging of mitochondrial nucleoids. Native nucleoids are not visible by EM using standard staining conditions. Immunogold staining with anti-DNA antibody has previously been used for EM visualization of nucleoids (Iborra et al., 2004), but the detergent or methanol permeabilization required to give the antibody access degrades cellular ultrastructure, and gold nanoparticles do not give the continuous staining that is necessary to outline the boundaries and other structural features of nucleoids.

Next, we sought to characterize the biotinylation activity of Twinkle-APEX2. Fluorescence imaging of HEK cells stably expressing Twinkle-APEX2, and treated with H_2O_2 for 1 min in the presence of biotin-phenol, showed a neutravidin-Alexa Fluor 647 signal (staining biotinylated proteins) that required the presence of both APEX and H_2O_2 (Figure 1E). The biotinylation pattern was tightly co-localized with the distribution of Twinkle-APEX2 itself, visualized by anti-V5 immunofluorescence, in most fields of view (Figure 1E). However, in other cells expressing Twinkle-APEX2 at higher levels, the biotinylation pattern filled the entire mitochondrial matrix while Twinkle-APEX2 remained punctate (Figure S1E). We have observed similar results before using other APEX2 fusion constructs, including IMS-APEX (Hung et al., 2014), APEX2-OMM (Lam et al., 2015), and ERM-APEX2 (Lam et al., 2015); despite giving diffuse biotinylation patterns by imaging, these constructs nevertheless produced very spatially specific proteomes and/or western blotting results. We surmise that the spread of biotinylation signal represents not non-specific labeling, but rather diffusion of biotinylated proteins (or other species) away from APEX2 during the 1-min labeling window.

Streptavidin blot analysis of whole-cell lysate showed that Twinkle-APEX2 biotinylates numerous endogenous proteins across a range of molecular weights (Figure 1F). For comparison, we also ran lysate from HEK cells stably expressing mito-APEX2, a construct that targets APEX2 throughout the entire mitochondrial matrix. Although the biotinylation "fingerprints" look largely similar, there are subtle differences in relative band intensities suggesting that some endogenous proteins are preferentially biotinylated by Twinkle-APEX2 over mito-APEX2. We proceeded to enrich the biotinylated proteomes using streptavidin beads, and analyzed the eluates by gel and silver staining. Figure 1F shows that labeling with both Twinkle-APEX2 and mito-APEX2 results in recovery of many biotinylated proteins, whereas negative controls with untransfected cells or omission of H_2O_2 recover much less material.

Proteomic Mapping of the Mitochondrial Nucleoid

Previously, we showed that a "ratiometric" APEX tagging strategy improved the spatial specificity of protein identifications in the mitochondrial IMS, a compartment that is leaky to biotin phenoxyl radicals, due to porins in the OMM (Hung et al., 2014). In the ratiometric approach, for each detected protein we compare its extent of biotinylation by targeted peroxidase (e.g., Twinkle-APEX2) versus non-targeted peroxidase (e.g., mito-APEX2). If a protein is biotinylated more extensively by Twinkle-APEX2 than by mito-APEX2, we retain it for our proteome. If it is biotinylated more extensively by mito-APEX2 than by Twinkle-APEX2, we reject it; such proteins may be just outside the nucleoid, accessible to the biotin radical but not a true nucleoid protein.

Because the mitochondrial nucleoid lacks a membrane altogether, and is a nucleoprotein complex rather than an organelle, it represents an even greater challenge than the mitochondrial IMS in terms of spatial specificity. Thus we reasoned that it would be essential to use the ratiometric tagging approach. The design of our proteomic experiment is shown in Figure 2A. Two independent replicates each feature three samples: one labeled by Twinkle-APEX2; one labeled throughout the mitochondrial matrix by mito-APEX2; and one unlabeled negative control sample with APEX2 or H_2O_2 omitted. The two different negative controls ensure that we remove proteins that may be tagged by endogenous peroxidases or endogenous H_2O_2.

All six samples from both replicates were independently lysed, and their biotinylated proteomes extracted using streptavidin beads. Proteins were digested (while still on beads) to peptides with trypsin, then chemically tagged with MS-differentiable tandem mass tagging (TMT) labels. Thereafter the six samples were pooled and analyzed as a mixture by liquid chromatography-tandem MS.

In total, 2,685 unique proteins were detected by MS (Figure 2B). However, the vast majority of these were non-specific streptavidin bead binders, identifiable by their 126/128 or 129/131 TMT intensity ratios close to 1. To remove these from further consideration, we used the 126/128 and 129/131 TMT ratios of known mitochondrial (true positive list) and known non-mitochondrial (false-positive list) proteins to guide us to optimal 126/128 and 129/131 cutoffs, which we then applied to the entire dataset (Figures 2C and S2B, "Filter 1"). More than 220 proteins remained in each dataset. We then used the 126/127 and 129/130 TMT ratios to distinguish nucleoid proteins proximal to Twinkle-APEX2 from non-proximal proteins that were biotinylated by mito-APEX2 to a similar or greater extent than Twinkle-APEX2 (Figure 2C, "Filter 2"). Application of 126/127 and 129/130 TMT cutoffs reduced the size of each list to ~70 proteins. Another view of the data is shown in Figure 2D, where the 126/128 TMT ratio, reflecting biotinylation extent by Twinkle-APEX2, is plotted against the 126/127 TMT ratio, reflecting relative proximity to Twinkle-APEX2 versus mito-APEX2. As expected, known nucleoid proteins such as TFAM, SSBP1, and Twinkle itself are clustered in the top right quadrant. The TMT ratio cutoffs applied to the data (Filter 1 and Filter 2) are shown as dashed lines. Finally, the two filtered lists were intersected to arrive at a final mitochondrial nucleoid proteome of 37 proteins (Figures 2B and 2C).

Characterization of Proteomic Dataset

To assess the specificity of our nucleoid proteome, we first analyzed mitochondrial annotation. All 37 of our proteins are known mitochondrial proteins, not cytosolic or nuclear contaminants, which have been observed in all previous nucleoid MS studies (Figure S1A). To determine nucleoid specificity, we checked for nucleoid-related annotation in the literature, or detection in three of the highest-quality previous nucleoid MS datasets (Bogenhagen et al., 2008; Rajala et al., 2015; Wang and Bogenhagen, 2006). Thirty proteins, or 81% of our list, have a prior nucleoid link by these criteria (Figure 2E). By contrast, the entire mitochondrial proteome of 1,591 proteins, analyzed in the same way, has only 22% of proteins with a nucleoid link. Our proteomic dataset is therefore clearly enriched for proteins with nucleoid-related function.

To assess sensitivity, or depth of coverage, of our proteome, we manually assembled a list of 21 proteins with strong prior experimental evidence of nucleoid localization (Table S1, tab 5). We detected 13 (62%) of these proteins. Several of the proteins we did not detect, including HSPA9 (Alkhaja et al., 2012), DNAJA3 (Ahn et al., 2010), HADHA (Ushikubo et al., 1996), LRPPRC (Bogenhagen et al., 2008), and SUPV3L1 (Bogenhagen et al., 2008), are known to be dual-localized, with a nucleoid population as well as a non-nucleoid population in the mitochondrial matrix. As can be seen in Figure 2D, these proteins were strongly biotinylated by Twinkle-APEX2, but because their non-nucleoid populations were also strongly tagged by matrix-APEX2 they were filtered out on the basis of low 126/127 or 129/130 TMT ratio. This is a downside of the ratiometric tagging approach, which increases specificity at the expense of coverage. Our previous IMS proteome also excluded known dual-localized proteins (Hung et al., 2014).

Figure 2F illustrates some aspects of the specificity and coverage of our nucleoid proteome. We enriched all four essential components of mtDNA replication (the "minimal mtDNA replisome" [Korhonen et al., 2004]) and all three essential components of mtDNA transcription (Litonin et al., 2010). As we move away from mitochondrial genome-related activities to RNA processing and protein translation, we see fewer detected proteins. This pattern of detection suggests that spatial organization in the mitochondrial matrix mirrors function.

Our nucleoid proteome can also be compared with previous mammalian nucleoid MS datasets. Figure S1A shows that our dataset is the most specific, especially in comparison with studies that used crosslinking (Bogenhagen et al., 2008; He et al., 2012). Our coverage is identical to that of two previous studies (Rajala et al., 2015; Wang and Bogenhagen, 2006) and a bit lower than another (Bogenhagen et al., 2008). However, the Venn diagrams in Figure S1B suggest that the factors that limit our coverage may be different from the factors that limit coverage in previous studies. We miss many dual-localized proteins such as HSPA9, DNAJA3, and LRPPRC, for reasons explained above. The study by Wang and Bogenhagen (2006), on the other hand, misses proteins such as LONP1, POLDIP2, and MGME1, which may be weakly or transiently associated with the nucleoid and therefore removed by washing. Thus, APEX proximity labeling and immunoprecipitation/ fractionation appear to be complementary techniques, each able to retrieve unique sets of nucleoid proteins.

We were interested in probing more deeply the 19% of our proteomic list (seven proteins) without prior literature connection to nucleoids. These could be false positives or newly discovered nucleoid proteins. For follow-up validation of these proteins, we performed western blots of candidate proteins in purified nucleoid preparation or fluorescence microscopy with mtDNA co-stained, depending on the availability of antibodies and genetic constructs. For one "nucleoid orphan," the respiratory complex I assembly factor NDUFS6 (Kmita et al., 2015), western blotting revealed its presence in crosslinked nucleoids enriched by anti-V5 pull-down (from HEK 293T cells expressing TFAM-V5; Figure 2G). A second nucleoid orphan, C7ORF55, was analyzed by fluorescence imaging. Figure 2H shows that endogenous C7ORF55 overlaps with mtDNA puncta by 40%, while a negative control (MitoTracker) overlaps with mtDNA by only 27%.

These observations with NDUFS6 and C7ORF55 reinforce separate findings by other laboratories. Huttlin et al. (2015) showed that both NDUFS6 and C7ORF55 co-immunoprecipitate with LIG3, the major ligase involved in mtDNA base excision repair. Floyd et al. (2016) observed that C7ORF55 also interacts with nucleoid-related proteins POLDIP2, CLPX, and NT5DC2. It was previously known that NDUFS6 is an assembly factor for complex I (Kmita et al., 2015). Indirect evidence suggests that C7ORF55 may be an assembly factor for complex V: Lefebvre-Legendre et al. (2001) showed that the yeast homolog of C7ORF55 is a complex V (ATP synthase) assembly factor, and both Floyd et al. (2016) and Huttlin et al. (2015) reported that C7ORF55 interacts with ATPAF2, a complex V subunit, in human cells. Hence, the spatial assignment of NDUFS6 and C7ORF55 to the mitochondrial nucleoid by our study, combined with previous literature observations, suggests that these proteins may functionally (and perhaps physically) link OXPHOS assembly and function to mtDNA repair. Such a link might represent a cellular mechanism to mitigate DNA damage caused by OXPHOS-generated reactive oxygen species.

Finally, we performed fluorescence imaging on a third nucleoid orphan, FASTKD1. Figures 3A and 3B show that recombinant FASTKD1 also co-localizes with mtDNA (42% compared with 21% for a negative control). Thus, our followup experiments show that three of our seven nucleoid orphans are specific hits rather than false positives. The nucleoid specificity of 81% therefore represents a lower bound to the actual specificity of our dataset.

FASTKD1 Negatively Regulates ND3 Transcript Level and Complex I Function

FASTKD1 is a nucleoid orphan identified in our proteome, and Figures 3A and 3B show that it co-localizes with mtDNA by fluorescence microscopy. We were curious about the potential function of FASTKD1 in the mitochondrial nucleoid. FASTKD1 belongs to a family of six metazoan-specific proteins containing both FASTK (Fas-activated serine/threonine kinase-like) and RAP (~60-residue RNA binding domain abundant in Apicomplexans) domains. While the functions of the five other FASTK family members have been studied by knockdown (Antonicka and Shoubridge, 2015; Jourdain et al., 2015; Simarro et al., 2010; Wolf and Mootha, 2014), FASTKD1 has not previously been examined.

Due to the presence of an RNA binding domain within FASTKD1, we used qRT-PCR to examine the effects of FASTKD1 knockdown on all 13 mRNA and two rRNA transcripts encoded by the mitochondrial genome. Figure 3C shows that the abundance of one specific

transcript, ND3, is strikingly increased upon FASTKD1 depletion. This is unlikely to be an off-target effect, because an alternative small hairpin RNA (shRNA) targeting a different region of the FASTKD1 gene produced the same phenotype (Figure S3A). To find out whether the effect was at the RNA level rather than a consequence of changes in mtDNA abundance, we used qPCR to measure mtDNA abundance in FASTKD1 knockdown cells. Figure 3D shows no difference in mtDNA levels in these cells compared with control shRNA-treated cells.

ND3 is a subunit of complex I, the first complex of the mitochondrial electron transport chain that transfers electrons from NADH to ubiquinone. If FASTKD1 is a negative regulator of ND3 mRNA, as suggested by our RT-PCR data in Figure 3C, then FASTKD1 may also indirectly influence the protein levels and enzymatic activity of complex I overall. To test this hypothesis, we lysed FASTKD1 knockdown cells and blotted for endogenous components of complex I. Figure 3E shows that both NDUFB8 and NDUFS6 protein subunits within complex I increase by ~ 1.8- and 1.6-fold compared with lysates from control shRNA cells. Markers for the other complexes, complexes II–V, do not change upon FASTKD1 knockdown, indicating that its effect on the electron transport chain is specific for complex I.

We also examined complex I activity using a commercial assay for NADH consumption. Figure 3F shows that FASTKD1 knockdown increases complex I activity by ~1.7-fold compared with control shRNA cells. By contrast, FASTKD1 knockdown causes no change in the activity of complex II, whose subunits are encoded by the nuclear genome.

Given that other members of the FASTK protein family have been implicated in mitochondrial mRNA binding, it is not surprising that FASTKD1 also plays a role in mitochondrial mRNA regulation. However, it is unique and without precedent that FASTKD1 is a specific *negative* regulator of ND3 mRNA. FASTK, FASKD2, FASTKD4, and FASTKD5, for example, are all positive regulators of specific mitochondrial mRNAs (Antonicka and Shoubridge, 2015; Jourdain et al., 2015; Simarro et al., 2010; Wolf and Mootha, 2014). Complex I is the least abundant complex of the electron transport chain (Schagger and Pfeiffer, 2001). Complex I transcripts are also known to have the shortest half-lives (Nagao et al., 2008). FASTKD1 may help regulate complex I levels in the mitochondrion, acting on nascent ND3 mRNA generated at the mitochondrial nucleoid.

DISCUSSION

In previous work, we used APEX-based proximity biotinylation to map two submitochondrial proteomes, the mitochondrial matrix and IMS. Here, our focus was on a smaller and more specialized subcompartment of the mitochondrion, the nucleoid that houses the mitochondrial genome. By studying this compartment, we have pushed the boundaries of APEX methodology, analyzing a non-membrane-enclosed dynamic nucleoprotein complex.

Although the nucleoid proteome has previously been analyzed by MS, the imperfect nature of biochemical fractionation led to considerable numbers of false positives (Bogenhagen et

al., 2008), false negatives (Rajala et al., 2015), or both (He et al., 2012) (Figure S1A). APEX represents an orthogonal and complementary approach. Instead of purifying the macromolecular complex, we covalently tag its components in living cells for subsequent identification by MS.

To illustrate the complementarity between diverse approaches, when we combine our dataset with the immunoprecipitation-based dataset of Wang and Bogenhagen (2006) a striking 80% of expected nucleoid proteins are recovered, higher than any one dataset alone.

As discussed above, our nucleoid proteome is missing dual-localized proteins because they are filtered out by the nucleoid-APEX/matrix-APEX signal intensity ratios that we use to enhance our specificity. However, it is possible to generate from the MS data a second list of potential dual-localized nucleoid proteins (Table S1, tab 3). These 23 proteins were strongly biotinylated by *both* Twinkle-APEX2 and mito-APEX2. Although we expect the false-positive rate of this list to be higher, it nevertheless contains some interesting candidate proteins and several of the well-established nucleoid proteins that were already known to be dual-localized (e.g., LRPPRC, HSPA9, CLPX, and HADHA).

Another methodological contribution of our study is the use of APEX for EM visualization of mitochondrial nucleoids. In contrast to fluorescence, a major advantage of EM is that endogenous context is visible. Without having to co-transfect or co-stain for separate markers, we can observe the spatial relationship of the mitochondrial nucleoid to the mitochondrial inner membrane, outer membrane, cristae, and cristae junctions. Other organellar membranes are also visible, such as the ER. Consistent with other studies (Kornmann et al., 2009; Lewis et al., 2016), preliminary analysis of our EM data from HEK 293T cells suggests that a substantially larger fraction of nucleoids co-localize with mitochondria-ER contact sites than would be expected if the nucleoids were randomly distributed throughout the matrix (Figure S1G).

Due to its high specificity, the proteome of 37 nucleoid proteins we generated by APEX mapping has biological value. For example, it led us to discover (and validate) NDUFS6, C7ORF55, and FASTKD1 as three novel nucleoid proteins. Our subsequent knockdown studies on FASTKD1 highlighted a role in specific negative regulation of ND3 mRNA levels, which in turn affects complex I protein levels. Our preliminary data raise further questions regarding the mechanism of ND3 mRNA regulation, and how control of this single transcript affects levels of other proteins within complex I, which has 45 subunits.

Our nucleoid proteome can also serve as a resource for generation of novel hypotheses. For example, there is ongoing discussion and debate regarding the spatial location of RNA processing of newly synthesized transcripts. Bogenhagen et al. (2014) have suggested that RNA processing and ribosome assembly occur at the nucleoid. However, other groups find evidence for RNA granules and processing of polycistronic transcripts into mature mtRNA at distinct foci away from mitochondrial nucleoids (Antonicka et al., 2013; Jourdain et al., 2013). Our proteomic dataset includes 12 RNA binding and processing enzymes, including the core components of mitochondrial RNA granules (GRSF1, TRMT10C, and DHX30) and ERAL1, which specifically binds to 12S mitochondrial rRNA (Dennerlein et al., 2010). We

note that GRSF1, TRMT10C, and ERAL1 were all detected in a previous crosslinked nucleoid preparation (Bogenhagen et al., 2008), but were not known to be mitochondrial proteins at the time and therefore discarded as contaminants; this highlights the importance of acquiring proteomic datasets with low false discovery rates. The appearance of such a large number of RNA-associated proteins in our nucleoid dataset lends support to the notion that RNA processing begins at mitochondrial nucleoids, and that RNA granules are dynamic physical extensions of the nucleoids, as proposed by Bogenhagen et al. (2014).

A second hypothesis inspired by our dataset concerns potential molecular crosstalk between mtDNA replication or maintenance and one-carbon metabolism. We enriched three of the four major enzymes in the mitochondrial folate pathway (SHMT2, MTHFD2, MTHFD1L, ALDH1L2) (Nilsson et al., 2014) (Figure 2C). Although SHMT2 was already a known nucleoid protein (Anderson et al., 2011; Bogenhagen et al., 2008; Wang and Bogenhagen, 2006) and MTHFD1L is upregulated in mouse models with mtDNA replication defects (Nikkanen et al., 2016), our dataset newly connects ALDH1L2 and MTHFD1L to mtDNA. Perhaps these enzymes in the folate cycle, which contribute to nucleotide synthesis, enable crosstalk between mtDNA replication status and cellular dinucleotide triphosphate pools.

Our proteome can also be utilized for biology in other ways. For several of the proteins we enrich (IVD, IDH2, ABHD10, GRPEL2, PDSS2), the only prior evidence for nucleoid localization was detection in previous crosslinked nucleoid MS studies. IDH2 is especially intriguing as its yeast homolog is known to be a key interaction partner of Abf2 (Kucej et al., 2008) (the yeast homolog of TFAM) and specifically binds to 5′ UTRs of yeast mtRNAs (Elzinga et al., 1993). Interaction of metabolic proteins with mtDNA has been of great interest since the initial report by Butow's group that aconitase binds to mtDNA (Chen et al., 2005).

In summary, our study extends APEX proteomic mapping to membrane-free macromolecular complexes in living cells, and produces an inventory of mtDNA-localized nucleoid proteins. This proteomic dataset extends the specificity and coverage of previous MS-based datasets, enabling new observations and hypotheses.

SIGNIFICANCE

Characterization of protein content within macromolecular complexes is central to understanding protein interaction networks and cellular organization. Here, we apply a protein labeling technique based on an engineered ascorbate peroxidase (APEX) to map the proteins associated with mtDNA in living cells. Our resulting proteome demonstrates that APEX labeling has the spatial resolution for mapping non-membrane delimited macromolecular complexes with high specificity, and provides a resource for systematic functional analysis of the mitochondrial nucleoid. Furthermore, we show that FASTKD1, an mtDNA-associated protein newly identified in our study, negatively regulates respiratory complex I abundance and activity by specifically repressing complex I subunit ND3 transcripts. These observations highlight the potential of applying APEX labeling to macromolecular complexes to reveal new biology.

EXPERIMENTAL PROCEDURES

Mammalian Cell Culture—HEK-293T, HeLa, or COS-7 cells from the ATCC (passages <25) were cultured in a 1:1 DMEM/MEM mixture (Cellgro) supplemented with 10% fetal bovine serum, 50 units/mL penicillin, and 50 μg/mL streptomycin at 37°C under 5% CO_2. Mycoplasma testing was not performed before experiments. For fluorescence microscopy imaging experiments, cells were grown on 7×7-mm glass coverslips in 48-well plates. For EM imaging experiments, HEK293T cells were grown on 35-mm glass-bottomed Petri dishes (MatTek). To improve the adherence of HEK293T cells, we pretreated glass slides with 50 μg/mL fibronectin (Millipore) for 20 min at 37°C before cell plating and washing three times with Dulbecco's PBS (DPBS) (pH 7.4).

Generation of Stable Twinkle-APEX2 and Mito-APEX2 HEK 293T Cells—For preparation of lentiviruses, HEK293T cells in 6-well plates were transfected at ~60%–70% confluency with the lentiviral vector pLX304 containing the gene of interest (1,000 ng), the lentiviral packaging plasmids dR8.91 (900 ng) and pVSV-G (100 ng), and 8 μL of Lipofectamine 2000 for 4 hr. About 60 hr after transfection the cell medium containing lentivirus was harvested and filtered through a 0.45-μm filter. HEK 293T cells were then infected at ~50% confluency, followed by selection with 8 μg/mL blasticidin in growth medium for 7 days before further analysis.

Biotin-Phenol Labeling in Live Cells—For imaging of HEK 293T cells stably expressing Twinkle-APEX2 or mito-APEX2, biotin-phenol labeling was initiated by changing the medium to fresh medium containing 500 mM biotin-phenol. This was incubated at 37°C under 5% CO_2 for 30 min. H_2O_2 was then added to each well for a final concentration of 1 mM H_2O_2, and the plate gently agitated for 1 min. The reaction was quenched by replacing the medium with an equal volume of 5 mM Trolox and 10 mM sodium ascorbate in DPBS. Cells were washed with DPBS containing 5 mM Trolox and 10 mM sodium ascorbate three times before proceeding to western blotting or imaging experiments.

Streptavidin Bead Enrichment of Biotinylated Material—HEK293T cells expressing the indicated APEX fusion constructs were labeled with biotin-phenol as described above. Cell pellets were then lysed in RIPA lysis buffer, 1 mM PMSF, 5 mM Trolox, 10 mM sodium ascorbate, and 10 mM sodium azide. The lysates were cleared by centrifugation at $15,000 \times g$ for 10 min at 4°C. Streptavidin-coated magnetic beads (Pierce) were washed twice with RIPA buffer, and 8 mg of each sample was separately incubated with 600 μL of magnetic bead slurry with rotation for 1 hr at room temperature or overnight at 4°C. The beads were subsequently washed twice with 1 mL of RIPA lysis buffer, once with 1 mL of 1 M KCl, once with 1 mL of 0.1 M Na_2CO_3, once with 1 mL of 2 M urea in 10 mM Tris-HCl (pH 8.0), and twice with 1 mL RIPA lysis buffer. For streptavidin blot analysis, biotinylated proteins were then eluted by boiling the beads in 75 μL of 3× protein loading buffer supplemented with 20 mM DTT and 2 mM biotin, and run on SDS-PAGE gel.

shRNA Knockdown of FASTKD1—Two FASTKD1 shRNAs (shRNA1 and shRNA2) and a non-targeting control shRNA (Table S2) were separately cloned into a lentiviral vector

pLKO.1 (Addgene). For preparation of lentiviruses, HEK-293T cells in 6-well plates were transfected at ~60%–70% confluency with the indicated pLKO.1 construct (1,000 ng), the lentiviral packaging plasmids dR8.91 (900 ng) and pVSV-G (100 ng), and 8 μL of Lipofectamine 2000 for 4 hr. About 60 hr after transfection the cell medium containing lentivirus was harvested and filtered through a 0.45-μm filter. HEK 293T cells were then infected at ~50% confluency, selected with 1 μg/mL puromycin in growth medium for 7 days, and left to recover in normal medium for 24–48 hr before further analysis.

mtDNA Copy Number Assay—Total DNA from the indicated HEK 293T cell lines were extracted with DNeasy kit (Qiagen) and diluted to 10 ng/μL. The relative level of mtDNA was then measured exactly as described previously (Kitami et al., 2012). MT-ND2 Taqman probe mix (900 nM primers, 250 nM probe) and Alu Taqman probe mix (1,000 nM primers, 100 nM probe) were mixed together with Taqman universal PCR master mix (Applied Biosystems) according to the manufacturer's protocol. MT-ND2 refers to mtDNA sequence and Alu is a human repeat sequence in the nuclear DNA. All sequences are listed in Table S3. Data were acquired and analyzed on an Applied Biosystems StepOnePlus Real-Time PCR Systems instrument (Figures 3D and S1F).

Real-Time PCR Assay—Total RNA from the indicated HEK 293T cell lines was extracted using an RNeasy Mini kit (Qiagen). Genomic DNA was digested with RNase-Free DNase (Qiagen), and 1,000 ng of total RNA was reverse transcribed using a SuperScript III Reverse Transcriptase kit (Thermo Fisher Scientific) with random hexamers (Thermo Fisher Scientific). The relative quantity of cDNA was measured using SYBR Green PCR master mix (Applied Biosystems) according to the manufacturer's protocol (Figures 3C, S3A, and S3B). qRT-PCR primer sequences are listed in Table S3. All data were acquired and analyzed on an Applied Biosystems StepOnePlus Real-Time PCR Systems instrument.

Complex I and II Activity Assay—Complex I activity was assayed using a complex I enzyme activity dipstick assay kit (Abcam Mitosciences). Complex II activity was assayed using a complex II enzyme activity microplate kit (Abcam Mitosciences). A standard curve was generated before the actual experiment was performed. Control shRNA cells and FASTKD1 shRNA cells were plated in 6-well plates and then scraped and pelleted by centrifugation at $3,000 \times g$ for 10 min. Cell pellets were lysed according to the manufacturer's protocol and protein concentration was quantified by bicinchoninic acid assay to ensure equal loading between samples. For complex I assay, 7 μg of protein from whole-cell lysate was used for each sample. Band intensities were quantified using ImageJ software. For complex II assay, 70 μg of protein from whole-cell lysate was used for each sample. Absorbance at 600 nm was measured using a plate reader.

Transfection and Immunofluorescence Staining—For transfection of the plasmids (see Table S2), cells plated on 7×7-mm glass coverslips in 48-well plates were transfected at ~50%–60% confluency with 100 ng of the corresponding plasmids and 1 μL of Lipofectamine 2000 for 4 hr. MitoTracker (Life Technologies) labeling was performed according to the manufacturer's protocol (Figures 2H and S2C). Twenty-four hours after transfection, cells were fixed with 4% paraformaldehyde in PBS at room temperature for 10

min. Cells were then washed with PBS three times and permeabilized with cold methanol at −20°C for 5 min. Cells were washed again three times with PBS and blocked for 1 hr with 3% BSA in PBS ("blocking buffer") at room temperature. Cells were then incubated with primary antibodies (see Supplemental Experimental Procedures) in blocking buffer for 1 hr at room temperature. After washing three times with PBS, cells were incubated with secondary antibodies in blocking buffer for 30 min. Cells were then washed three times with PBS and imaged.

Immunoprecipitation of Crosslinked Nucleoids—HEK 293T cells expressing TFAM-V5 or mito-GFP-V5 were treated with 1% formaldehyde in DPBS for 10 min at room temperature for crosslinking. The reaction was stopped by addition of 125 mM glycine (pH 8.0; final concentration), and cells were subsequently lysed in TENT buffer (50 mM Tris-HCl pH 7.4, 300 mM NaCl, 2 mM EDTA, and 1% Triton X-100). Crosslinked material from 350 mg of whole-cell lysate was immunoprecipitated with 25 μL of Dynabeads protein G (Thermo Fisher) and mouse anti-V5 antibody (Life Technologies, 1:100 dilution). Beads were then washed three times with TENT buffer, boiled for 10 min, and eluted with 33 protein loading buffer. Protein samples were then boiled for 50 min at 95°C to reverse formaldehyde crosslinks and then subjected to SDS-PAGE.

Gels and Western Blots—HEK 293T cells stably expressing the indicated constructs were plated in 6-well plates and scraped and pelleted by centrifugation at $3,000 \times g$ for 10 min. The pellet was stored at −80°C and lysed with RIPA lysis buffer (50 mM Tris, 150 mM NaCl, 0.1% SDS, 0.5% sodium deoxycholate, 1% Triton X-100, 1× protease cocktail [Sigma-Aldrich], and 1 mM PMSF) for 5 min at 4°C. The cell pellet was resuspended by gentle pipetting. Lysates were clarified by centrifugation at $15,000 \times g$ for 10 min at 4°C before separation on an SDS-PAGE gel. Silver-stained gels (Figure 1F) were generated using a silver stain kit (Pierce). Gels were transferred to nitrocellulose membrane, stained by Ponceau S (10 min in 0.1% [w/v] Ponceau S in 5% acetic acid/water). The blots were then blocked and stained with primary and secondary antibodies as described in Supplemental Experimental Procedures.

Supplementary Material

Refer to Web version on PubMed Central for supplementary material.

Acknowledgments

References

Ahn BY, Trinh DLN, Zajchowski LD, Lee B, Elwi AN, Kim SW. Tid1 is a new regulator of p53 mitochondrial translocation and apoptosis in cancer. Oncogene. 2010; 29:1155–1166. [PubMed: 19935715]

Alkhaja AK, Jans DC, Nikolov M, Vukotic M, Lytovchenko O, Ludewig F, Schliebs W, Riedel D, Urlaub H, Jakobs S, et al. MINOS1 is a conserved component of mitofilin complexes and required for mitochondrial function and cristae organization. Mol Biol Cell. 2012; 23:247–257. [PubMed: 22114354]

Anderson DD, Quintero CM, Stover PJ. Identification of a de novo thymidylate biosynthesis pathway in mammalian mitochondria. Proc Natl Acad Sci USA. 2011; 108:15163–15168. [PubMed: 21876188]

Antonicka H, Shoubridge EA. Mitochondrial RNA granules are centers for posttranscriptional RNA processing and ribosome biogenesis. Cell Rep. 2015; 10:920–932.

Antonicka H, Sasarman F, Nishimura T, Paupe V, Shoubridge EA. The mitochondrial RNA-binding protein GRSF1 localizes to RNA granules and is required for posttranscriptional mitochondrial gene expression. Cell Metab. 2013; 17:386–398. [PubMed: 23473033]

Bogenhagen DF, Rousseau D, Burke S. The layered structure of human mitochondrial DNA nucleoids. J Biol Chem. 2008; 283:3665–3675. [PubMed: 18063578]

Bogenhagen DF, Martin DW, Koller A. Initial steps in RNA processing and ribosome assembly occur at mitochondrial DNA nucleoids. Cell Metab. 2014; 19:618–629. [PubMed: 24703694]

Brown TA, Tkachuk AN, Shtengel G, Kopek BG, Bogenhagen DF, Hess HF, Clayton DA. Superresolution fluorescence imaging of mitochondrial nucleoids reveals their spatial range, limits, and membrane interaction. Mol Cell Biol. 2011; 31:4994–5010. [PubMed: 22006021]

Chen XJ, Wang X, Kaufman BA, Butow RA. Aconitase couples metabolic regulation to mitochondrial DNA maintenance. Science. 2005; 307:714–717. [PubMed: 15692048]

Copeland WC. Defects in mitochondrial DNA replication and human disease. Crit Rev Biochem Mol Biol. 2012; 47:64–74. [PubMed: 22176657]

Dennerlein S, Rozanska A, Wydro M, Chrzanowska-Lightowlers ZMA, Lightowlers RN. Human ERAL1 is a mitochondrial RNA chaperone involved in the assembly of the 28S small mitochondrial ribosomal subunit. Biochem J. 2010; 430:551–558. [PubMed: 20604745]

Elzinga SD, Bednarz AL, van Oosterum K, Dekker PJ, Grivell LA. Yeast mitochondrial NAD(+)-dependent isocitrate dehydrogenase is an RNA-binding protein. Nucleic Acids Res. 1993; 21:5328–5331. [PubMed: 7505425]

Floyd BJ, Wilkerson EM, Veling MT, Minogue CE, Xia C, Beebe ET, Wrobel RL, Cho H, Kremer LS, Alston CL, et al. Mitochondrial protein interaction mapping identifies regulators of respiratory chain function. Mol Cell. 2016; 63:621–632. [PubMed: 27499296]

Gilkerson R, Bravo L, Garcia I, Gaytan N, Herrera A, Maldonado A, Quintanilla B. The mitochondrial nucleoid: integrating mitochondrial DNA into cellular homeostasis. Cold Spring Harb Perspect Biol. 2013; 5:a011080. [PubMed: 23637282]

He J, Cooper HM, Reyes A, Di Re M, Sembongi H, Litwin TR, Gao J, Neuman KC, Fearnley IM, Spinazzola A, et al. Mitochondrial nucleoid interacting proteins support mitochondrial protein synthesis. Nucleic Acids Res. 2012; 40:6109–6121. [PubMed: 22453275]

Hung V, Zou P, Rhee HW, Udeshi ND, Cracan V, Svinkina T, Carr SA, Mootha VK, Ting AY. Proteomic mapping of the human mitochondrial intermembrane space in live cells via ratiometric APEX tagging. Mol Cell. 2014; 55:332–341. [PubMed: 25002142]

Huttlin EL, Ting L, Bruckner RJ, Gebreab F, Gygi MP, Szpyt J, Tam S, Zarraga G, Colby G, Baltier K, et al. The BioPlex network: a systematic exploration of the human interactome. Cell. 2015; 162:425–440. [PubMed: 26186194]

Iborra FJ, Kimura H, Cook PR. The functional organization of mitochondrial genomes in human cells. BMC Biol. 2004; 2:9. [PubMed: 15157274]

Jourdain AA, Koppen M, Wydro M, Rodley CD, Lightowlers RN, Chrzanowska-Lightowlers ZM, Martinou JC. GRSF1 regulates RNA processing in mitochondrial RNA granules. Cell Metab. 2013; 17:399–410. [PubMed: 23473034]

Jourdain AA, Koppen M, Rodley CD, Maundrell K, Gueguen N, Reynier P, Guaras AM, Enriquez JA, Anderson P, Simarro M, et al. A mitochondria-specific isoform of FASTK is present in mitochondrial RNA granules and regulates gene expression and function. Cell Rep. 2015; 10:1110–1121. [PubMed: 25704814]

Kaufman BA, Newman SM, Hallberg RL, Slaughter CA, Perlman PS, Butow RA. In organello formaldehyde crosslinking of proteins to mtDNA: identification of bifunctional proteins. Proc Natl Acad Sci USA. 2000; 97:7772–7777. [PubMed: 10869431]

Kitami T, Logan DJ, Negri J, Hasaka T, Tolliday NJ, Carpenter AE, Spiegelman BM, Mootha VK. A chemical screen probing the relationship between mitochondrial content and cell size. PLoS One. 2012; 7:e33755. [PubMed: 22479437]

Kmita K, Wirth C, Warnau J, Guerrero-Castillo S, Hunte C, Hummer G, Kaila VRI, Zwicker K, Brandt U, Zickermann V. Accessory NUMM (NDUFS6) subunit harbors a Zn-binding site and is essential for biogenesis of mitochondrial complex I. Proc Natl Acad Sci USA. 2015; 112:5685–5690. [PubMed: 25902503]

Kopek BG, Shtengel G, Xu CS, Clayton DA, Hess HF. Correlative 3D superresolution fluorescence and electron microscopy reveal the relationship of mitochondrial nucleoids to membranes. Proc Natl Acad Sci USA. 2012; 109:6136–6141. [PubMed: 22474357]

Korhonen JA, Pham XH, Pellegrini M, Falkenberg M. Reconstitution of a minimal mtDNA replisome in vitro. EMBO J. 2004; 23:2423–2429. [PubMed: 15167897]

Kornmann B, Currie E, Collins SR, Schuldiner M, Nunnari J, Weissman JS, Walter P. An ER-mitochondria tethering complex revealed by a synthetic biology screen. Science. 2009; 325:477–481. [PubMed: 19556461]

Kucej M, Kucejova B, Subramanian R, Chen XJ, Butow RA. Mitochondrial nucleoids undergo remodeling in response to metabolic cues. J Cell Sci. 2008; 121:1861–1868. [PubMed: 18477605]

Lam SS, Martell JD, Kamer KJ, Deerinck TJ, Ellisman MH, Mootha VK, Ting AY. Directed evolution of APEX2 for electron microscopy and proximity labeling. Nat Methods. 2015; 12:51–54. [PubMed: 25419960]

Lefebvre-Legendre L, Vaillier J, Benabdelhak H, Velours J, Slonimski PP, di Rago JP. Identification of a nuclear gene (FMC1) required for the assembly/stability of yeast mitochondrial F(1)-ATPase in heat stress conditions. J Biol Chem. 2001; 276:6789–6796. [PubMed: 11096112]

Lewis SC, Uchiyama LF, Nunnari J. ER-mitochondria contacts couple mtDNA synthesis with mitochondrial division in human cells. Science. 2016; 353:aaf5549. [PubMed: 27418514]

Litonin D, Sologub M, Shi Y, Savkina M, Anikin M, Falkenberg M, Gustafsson CM, Temiakov D. Human mitochondrial transcription revisited: only TFAM and TFB2M are required for transcription of the mitochondrial genes in vitro. J Biol Chem. 2010; 285:18129–18133. [PubMed: 20410300]

Loh KH, Stawski PS, Draycott AS, Udeshi ND, Lehrman EK, Wilton DK, Svinkina T, Deerinck TJ, Ellisman MH, Stevens B, et al. Proteomic analysis of unbounded cellular compartments: synaptic clefts. Cell. 2016; 166:1295–1307.e21. [PubMed: 27565350]

Martell JD, Deerinck TJ, Sancak Y, Poulos TL, Mootha VK, Sosinsky GE, Ellisman MH, Ting AY. Engineered ascorbate peroxidase as a genetically encoded reporter for electron microscopy. Nat Biotechnol. 2012; 30:1143–1148. [PubMed: 23086203]

Nagao A, Hino-Shigi N, Suzuki T. Measuring mRNA decay in human mitochondria. Methods Enzymol. 2008; 447:489–499. [PubMed: 19161857]

Nikkanen J, Forsström S, Euro L, Paetau I, Kohnz RA, Wang L, Chilov D, Viinamäki J, Roivainen A, Marjamäki P, et al. Mitochondrial DNA replication defects disturb cellular dNTP pools and remodel one-carbon metabolism. Cell Metab. 2016; 23:635–648. [PubMed: 26924217]

Nilsson R, Jain M, Madhusudhan N, Sheppard NG, Strittmatter L, Kampf C, Huang J, Asplund A, Mootha VK. Metabolic enzyme expression highlights a key role for MTHFD2 and the mitochondrial folate pathway in cancer. Nat Commun. 2014; 5:3128. [PubMed: 24451681]

Rajala N, Gerhold JM, Martinsson P, Klymov A, Spelbrink JN. Replication factors transiently associate with mtDNA at the mitochondrial inner membrane to facilitate replication. Nucleic Acids Res. 2014; 42:952–967. [PubMed: 24163258]

Rajala N, Hensen F, Wessels HJ, Ives D, Gloerich J, Spelbrink JN. Whole cell formaldehyde cross-linking simplifies purification of mitochondrial nucleoids and associated proteins involved in mitochondrial gene expression. PLoS One. 2015; 10:e0116726. [PubMed: 25695250]

Rhee HW, Zou P, Udeshi ND, Martell JD, Mootha VK, Carr SA, Ting AY. Proteomic mapping of mitochondria in living cells via spatially restricted enzymatic tagging. Science. 2013; 339:1328–1331. [PubMed: 23371551]

Roux KJ, Kim DI, Raida M, Burke B. A promiscuous biotin ligase fusion protein identifies proximal and interacting proteins in mammalian cells. J Cell Biol. 2012; 196:801–810. [PubMed: 22412018]

Schagger H, Pfeiffer K. The ratio of oxidative phosphorylation complexes I-V in bovine heart mitochondria and the composition of respiratory chain supercomplexes. J Biol Chem. 2001; 276:37861–37867. [PubMed: 11483615]

Simarro M, Gimenez-Cassina A, Kedersha N, Lazaro JB, Adelmant GO, Marto JA, Rhee K, Tisdale S, Danial N, Benarafa C, et al. Fast kinase domain-containing protein 3 is a mitochondrial protein essential for cellular respiration. Biochem Biophys Res Commun. 2010; 401:440–446. [PubMed: 20869947]

Spelbrink JN, Li FY, Tiranti V, Nikali K, Yuan QP, Tariq M, Wanrooij S, Garrido N, Comi G, Morandi L, et al. Human mitochondrial DNA deletions associated with mutations in the gene encoding Twinkle, a phage T7 gene 4-like protein localized in mitochondria. Nat Genet. 2001; 28:223–231. [PubMed: 11431692]

Ushikubo S, Aoyama T, Kamijo T, Wanders RJ, Rinaldo P, Vockley J, Hashimoto T. Molecular characterization of mitochondrial trifunctional protein deficiency: formation of the enzyme complex is important for stabilization of both alpha- and beta-subunits. Am J Hum Genet. 1996; 58:979–988. [PubMed: 8651282]

Wang Y, Bogenhagen DF. Human mitochondrial DNA nucleoids are linked to protein folding machinery and metabolic enzymes at the mitochondrial inner membrane. J Biol Chem. 2006; 281:25791–25802. [PubMed: 16825194]

Wanrooij S, Goffart S, Pohjoismäki JLO, Yasukawa T, Spelbrink JN. Expression of catalytic mutants of the mtDNA helicase Twinkle and polymerase POLG causes distinct replication stalling phenotypes. Nucleic Acids Res. 2007; 35:3238–3251. [PubMed: 17452351]

Wolf AR, Mootha VK. Functional genomic analysis of human mitochondrial RNA processing. Cell Rep. 2014; 7:918–931. [PubMed: 24746820]

Highlights

- 1-min live labeling by APEX peroxidase tags human mitochondrial nucleoid proteome

- 37 proteins enriched, 30 (81%) with prior nucleoid annotation

- NDUFS6, C7ORF55, and FASTKD1 validated as novel mitochondrial nucleoid proteins

- FASTKD1 downregulates ND3 mRNA, in turn decreasing complex I abundance & activity
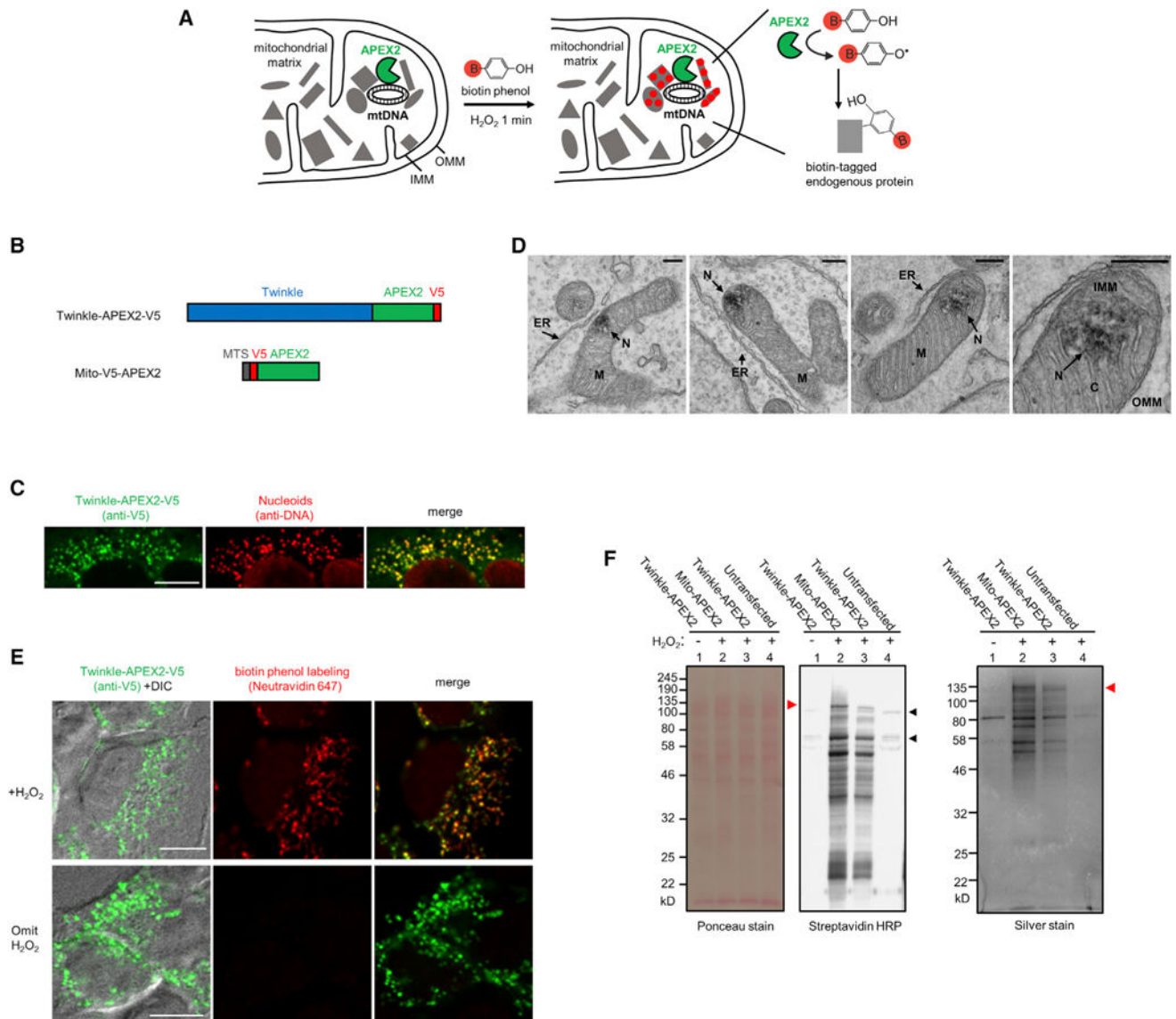
Figure 1. Design and Characterization of APEX2 Fusion Constructs Used for Live-Cell Proteomic Mapping

(A) Scheme of APEX2-mediated proximity biotinylation within the mitochondrial nucleoid. APEX2 (green) is genetically targeted to the nucleoid via fusion to Twinkle, a known nucleoid protein. The gray shapes are endogenous proteins residing inside and outside the nucleoid in the mitochondrial matrix. H_2O_2 is added for 1 min to cells preloaded with biotin-phenol (BP; red B = biotin) to initiate labeling. APEX2 oxidizes BP into a phenoxyl radical, which covalently tags proximal endogenous proteins at electron-rich side chains such as Tyr. mtDNA, mitochondrial DNA; OMM, outer mitochondrial membrane; IMM, inner mitochondrial membrane.

(B) APEX2 fusion constructs employed in this study. Mito-V5-APEX2 employs a 24-amino-acid mitochondrial targeting sequence (MTS) from COX4 to localize APEX2 throughout the entire mitochondrial matrix. V5 is an epitope tag.

(C) Fluorescence imaging of Twinkle-APEX2 localization. Stably expressed Twinkle-APEX2 (green) was visualized in HEK293T cells by anti-V5 staining (Alexa Fluor 647). Nucleoids (red) were visualized with anti-DNA antibody (Alexa Fluor 488). Figure S1D shows an expanded view of the entire cell. Scale bar, 10 μm.

(D) Electron microscopic (EM) visualization of stably expressed Twinkle-APEX2 in HEK293T cells. Dark-stained regions indicate APEX2 activity. Staining was performed after cell fixation with diaminobenzidine and H_2O_2 followed by reduced osmium. ER, endoplasmic reticulum; M, mitochondria; N, nucleoid; C, cristae. Scale bars, 200 nm.

(E) Fluorescence imaging of Twinkle-APEX2 activity. Live-cell biotinylation was performed for 1 min with BP and H_2O_2 as in (A). Cells were fixed and stained with anti-V5 antibody to visualize Twinkle-APEX2 (green, Alexa Fluor 488) and neutravidin-Alexa Fluor 647 (red) to visualize biotinylated proteins. DIC, differential interference contrast. Scale bars, 10 μm.

(F) Western blot analysis of biotinylated proteins from HEK 293T cells stably expressing the indicated APEX2 fusion construct and labeled with BP as in (A). Left: lysates were run on SDS-PAGE and analyzed by Ponceau staining or streptavidin blotting. Right: total eluted protein after streptavidin bead enrichment, visualized by silver staining. Lanes 1 and 4 are negative controls with H_2O_2 or APEX2 omitted, respectively. Black arrowheads point to endogenously biotinylated proteins. Red arrowheads point to proteins preferentially biotinylated by Twinkle-APEX2 over mito-APEX2.
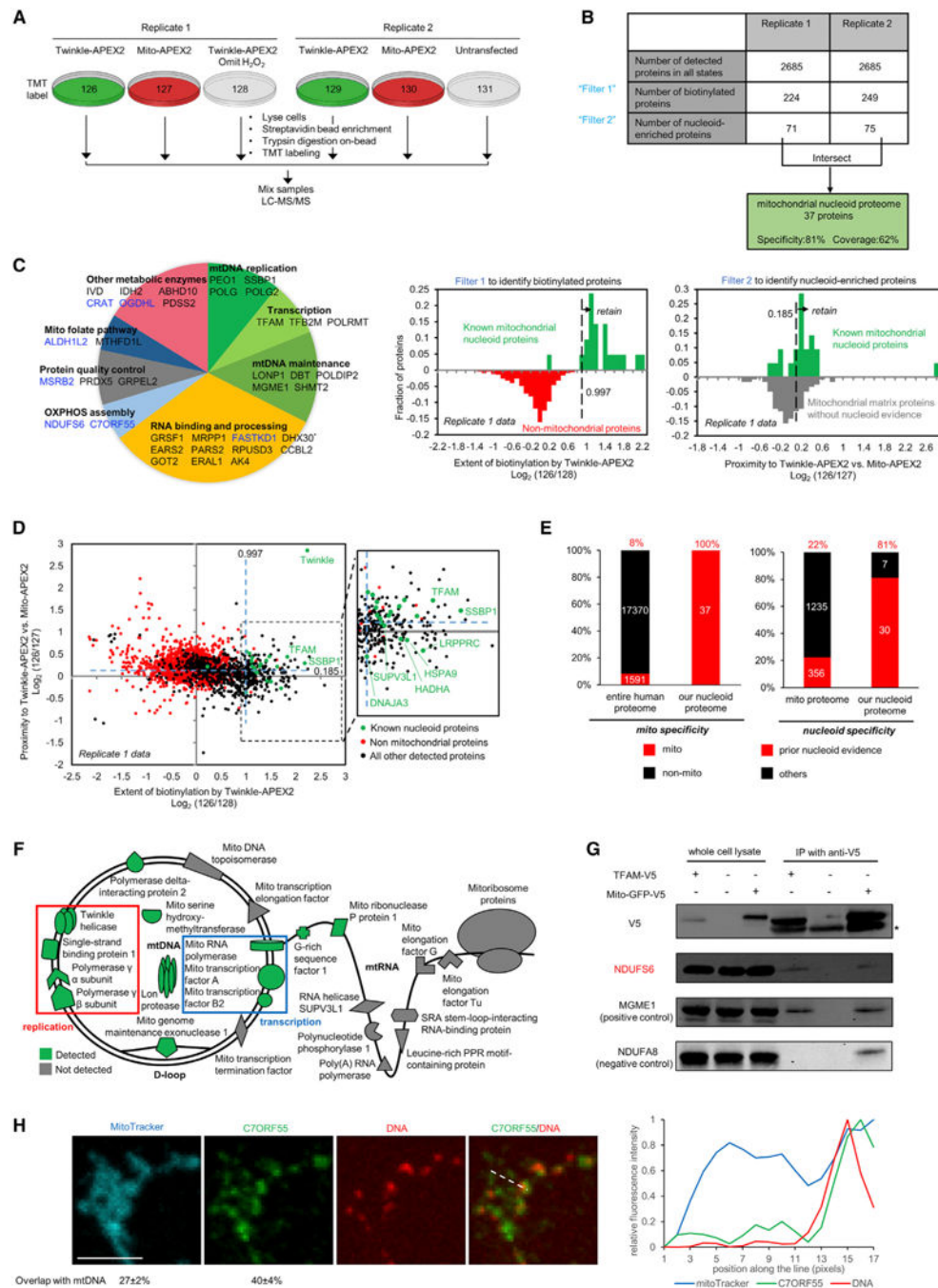
Figure 2. Acquisition and Analysis of Mitochondrial Nucleoid Proteomic Data

(A) Design of proteomic experiment. HEK293T cells stably expressing the indicated constructs were labeled with BP and H_2O_2 for 1 min, then lysed. Biotinylated proteins were enriched with streptavidin beads, then digested to peptides on-bead. Resulting peptides were chemically labeled with the indicated TMT labels. Samples were then combined as shown and analyzed by liquid chromatography and tandem MS.

(B) Filtering of MS data to produce the final mitochondrial nucleoid proteome. Table shows the number of proteins remaining after each filtering step. The two replicate datasets were

intersected to produce the final proteome. Scatterplots in Figure S2A show correlation between TMT ratios across replicates.

(C) Left: mitochondrial nucleoid proteome subdivided by protein functional class. Asterisk indicates that two isoforms of this protein are present in the proteome. Nucleoid orphans (proteins not previously linked to the mitochondrial nucleoid) are shown in blue. Right: histograms that illustrate how Filter 1 and Filter 2 cutoffs were determined. True positives (i.e., known mitochondrial nucleoid proteins) are plotted in the green histogram, and potential false positives are plotted in red or gray histograms. Receiver-operating characteristic analysis (Figure S2B) was applied to determine the TMT ratio cutoff value that maximized true positives while minimizing false positives.

(D) Graph of all proteins detected in Replicate 1, plotted by extent of biotinylation by Twinkle-APEX2 (x axis) and by relative proximity to Twinkle-APEX2 versus matrix-APEX2 (y axis). Known nucleoid proteins are colored green and non-mitochondrial proteins are colored red. Cutoffs determined in (C) and applied in (B) are shown as dashed blue lines. All five green dots below the horizontal dashed blue line are known to be dual-localized to the nucleoid and elsewhere in the mitochondrial matrix.

(E) Mitochondrial (left) and nucleoid (right) specificity of the proteomic list. Further details are provided in Table S1.

(F) Schematic showing well-established proteins related to the mitochondrial nucleoid, mitochondrial RNA processing, and protein translation. Proteins are colored according to their detection or lack of detection in our proteome. Red and blue rectangles enclose the minimal proteins sets required for reconstitution of mtDNA replication and transcription in vitro, respectively (Korhonen et al., 2004; Litonin et al., 2010).

(G) Western blot detection of nucleoid orphan NDUFS6 in purified nucleoids. HEK 293T cells expressing TFAM-V5 or mito-GFP-V5 were treated with formaldehyde, and crosslinked mitochondrial nucleoids were immunoprecipitated using anti-V5 antibody. Nucleoid protein MGME1 and OXPHOS protein NDUFA8 were also detected as positive and negative controls, respectively. Asterisk indicates the light chain of immunoglobulin G.

(H) Co-localization of endogenous C7ORF55 with mtDNA. Left: endogenous C7ORF55 (green, Alexa Fluor 488) was stained in HeLa cells together with mtDNA (red, Alexa Fluor 405). Mitochondria were visualized using MitoTracker (blue) labeling. Quantitation of MitoTracker and C7ORF55 overlap with mtDNA from 3 cells is shown as mean ± SD beneath the images. Figure S2C shows expanded view of the entire cell. Scale bar, 5 μm. Right: pixel intensity plot of the dashed line in image on the left.
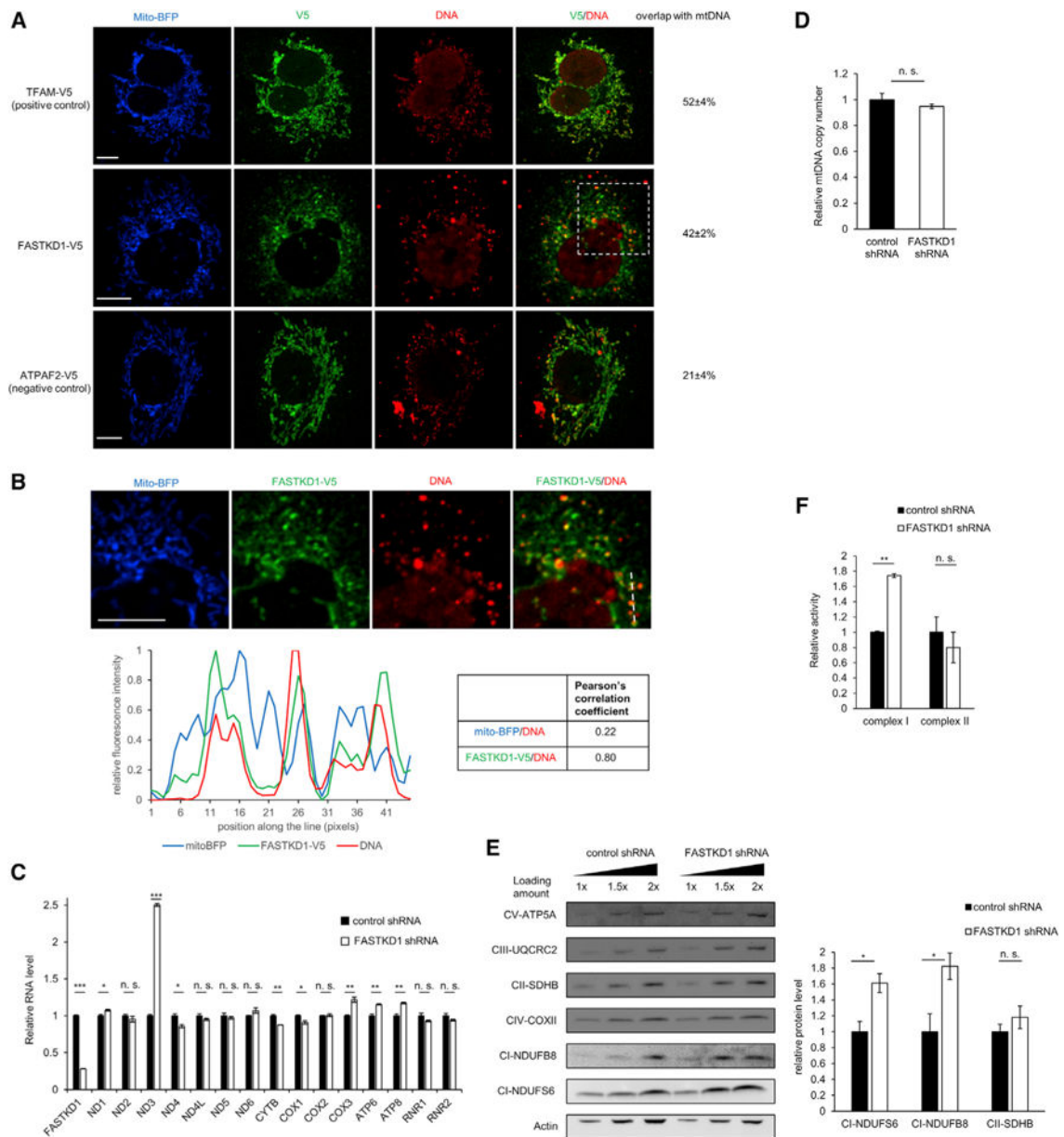
Figure 3. Expression of the ND3 Subunit of Complex I Is Specifically Regulated by FASTKD1

(A) Fluorescence imaging of FASTKD1-V5. COS-7 cells expressing the indicated constructs and mito-BFP (blue) were fixed and stained with anti-V5 antibody (green, Alexa Fluor 488) and anti-DNA antibody to visualize mtDNA (red, Alexa Fluor 647). Quantitation of V5 overlap with mtDNA from 3 cells is shown as mean ± SD on the right. TFAM-V5 and ATPAF2-V5 are positive and negative controls for nucleoid proteins, respectively. Scale bars, 10 μm.

(B) Co-localization of FASTKD1-V5 with mtDNA. Top: expanded view of the boxed region in (A). Scale bars, 10 μm. Bottom: pixel intensity plot of the dashed line shown in images above. Pearson's correlation coefficients for mitoBFP/DNA and V5/DNA are shown on the right.

(C) Relative abundance of FASTKD1 mRNA and each of the 15 other mitochondrial mRNAs and rRNAs encoded by the mitochondrial genome, in FASTKD1 shRNA knockdown cells versus controls. qRT-PCR data are shown as mean ± SEM (n = 3). Data were analyzed using a two-tailed Student's t test, with $*p < 0.05$, $**p < 0.01$, and $***p < 0.001$; n.s., not significant ($p > 0.05$).

(D) Relative mtDNA copy number in control shRNA knockdown cells compared with FASTKD1 shRNA knockdown cells, measured by qRT-PCR. Data are shown as mean ± SEM (n = 3). Data were analyzed using a two-tailed Student's t test, with n.s., not significant ($p > 0.05$).

(E) Western blot showing expression of complex I–V markers in FASTKD1 shRNA knockdown cells compared with control shRNA knockdown cells. Three different volumes of each cell lysate were loaded as indicated. Data from a replicate experiment shown in Figure S3C. Quantitation of complex I and II marker proteins (NDUFS6, NDUFB8, and SDHB) is shown on the right. Values are normalized to actin band intensities. Data are shown as mean ± SEM (n = 3) and analyzed using a two-tailed Student's t test, with $*p < 0.05$; n.s., not significant ($p > 0.05$).

(F) Relative respiratory complex I and complex II activities in control shRNA knockdown cells compared with FASTKD1 shRNA knockdown cells, measured by colorimetric assays. Equal amounts of lysate were loaded for each sample. Data are shown as mean ± SEM (n = 3) and analyzed using a two-tailed Student's t test, with $**p < 0.01$; n.s., not significant ($p > 0.05$).